RSC Advances

ROYAL SOCIETY OF CHEMISTRY

www.rsc.org/advances

A theoretical study on ionic liquid endohedral C540 fullerene

Gregorio García,[a] Mert Atilhan,[b] and S. Aparicio[*a]

[a] Department of Chemistry, University of Burgos, 09001 Burgos, Spain

[b] Department of Chemical Engineering, Qatar University, P.O. Box 2713, Doha, Qatar

[*]Corresponding author: sapar@ubu.es

Table of contents entry:

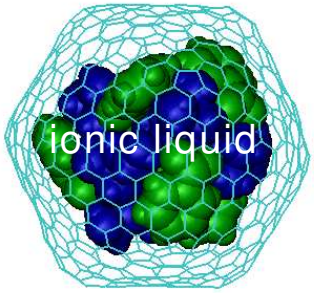

Abstract: The effect of the confinement of ionic liquid (choline benzoate) cluster inside of C540 fullerent has been studied through both molecular dynamic and density functional theory simulations. The solvation of the fullerene by the ionic liquid is also analysed and compared with pristine fullerene cages. The mobility of the studied endohedral fullerenes under external electric fields is simulated as a function of the intensity of the applied fields. Density Functional calculations allowed inferring both the changes in the electronic structure of C540 due to the ionic liquid and the interactions between the molecules forming the ionic liquid inside C540. This study is the first available study on endohedral fullerenes with confined ionic liquids published in open literature. More generally, theoretical simulations carried out in this work could be used both in the prediction of the properties and guide to the experimentalist to the rational desing of new materials based on ionic liquids confined in fullerenes for specific applications.

Keywords: ionic liquids; fullerene; endohedral; endofullerene, molecular dynamics; DFT; external electric field.

1. Introduction

Endohedral fullerenes (EHFs) are composed of fullerenes of different size encapsulating atoms, ions, molecules or molecular clusters.[1,2,3] The unconventional properties of these systems has attracted great attention in academia not only in physics and chemistry but also in such interdisciplinary areas as materials and biological sciences.[4,5,6,7] The possibility of isolating different atoms or molecules (e.g. metal atoms, nitrides, carbiedes , nobles gases or non metallic atoms) through their confinement in fullerene cages leads to the development of new platforms in searching novel functionalities and applications.[8,9,10] The main properties of all these types of EHFs and the state-of-the-art of the problem were recently reviewed by Popov et al.[3] The novel properties of most of the studied EHFs have make them as suitable options in fields as relevant as biomedicine,[11,12] or photovoltaics,[13] and possible applications in other fields such as lasers or superconductors have been considered.[3]

The encapsulation of molecules in fullerenes has led to a lower number of studies in comparison with metallofullerenes. Dodziuk et al.[14] reported a wide molecular mechanics study on EHFs formed by the encapsulation of small molecules (H_2, water), hydrocarbons, ketones, amines @ C60, C70, C76, C80 and C82 fullerenes, reporting the stabilization energy upon encapsulation and analysing the host-guest sizes in relationship with the stabilization upon confinement. Despite the simplicity of used computational approach, Dodziuk et al.[14] concluded the development of weak host-west interactions for most of the studied compounds. The confinement of H_2 clusters in C60 were studied theoretically by Ren et al.[15] and by Barajas-Barraza et al.,[16] analysing the molecular arrangement as a function of the dyhydrogen cluster sizing, respectively. Encapsulation of water molecules have led to several studies considering the incarceration of single water molecule,[17,18,19] but also of water clusters.[20,21] Charking et al.[22] analysed the properties of several guest molecules (e.g. benzene) in fullerenes using methods based on the density functional theory (DFT). DFT methods were also used by Ganji et al.[23] for the study of NH_3 confined at C60, considering not only single ammonia molecules but also the confinement of ammonia clusters. In spite of the attractive of using fullerene cages to isolate single molecules or molecular clusters of fixed size, studies on the confinement of more complex molecules are absent in the literature.

Ionic liquids (ILs) are compounds which have attracted great attention in the scientific community because of their remarkable physical and chemical properties,[24] the possibility of tuning these properties through a suitable combination of involved ions,[25,26] and their applications for very different technologies.[27,28] Therefore their behaviour with regard to

carbon nanostructures,[29,30] graphene,[31,32,33,34,35,36] carbon flakes,[37] graphene nanoribbons,[38,39] or nanopores arrays,[29,40] have been object of several works.The scarce literature on the behavior of fullerenes with ILs systems are mainly devoted to empty fullerene cages solvated in ILs.[39,41,42,43], Our research group used molecular dynamics simulations for the study of C60 solvated in the N-methylpiperazinium IL.[39] Nevertheless, up to our knowledge studies of ILs, or more complex molecules in general, confined inside fullerene cages (ionic liquid - EHFs) are absent in the literature.

Aimed to rational design new materials based on ILs confined in enhohedral fullenes for determinate tasks, a deeper knowledge on the influence of encapsulated molecules (guest) on the fullerene (host) features and viceversa is needed. Unfortunately, it is difficult to define a priori which molecules lead to concrete features. Up to now, a trial and error approach is widely used in experiments. This is a typical context wherein theoretical simulations can give new insights to experimentalist about the suitability of new systems. Thus, we propose here a computational study through both classical molecular dynamics (DM)and density functional theory (DFT) simulations on the characteristics of IL molecules confined inside of endohedral fullerenes. For this purpose, choline Benzoate IL (CH_BE, Figure 1) confined inside C540 fullerene was selected as a first case of study. Discarding classical ILscholine based cation ((2-hydroxyethyl)trimethylammonium) is among the most suitable new options for developing ILs due to the environmental, toxicological and economical aspects,[44,45,46] and the aromatic character of the selected anion. Moreover, our group reported a recent study on the behaviour of CH_BE with regard to graphene and single-walled carbon nanotubes.[36] Beyond, to study the confinenement of single ion or single IL molecule inside a fullerene cage, we decided to study the confinement of several IL molecules. Therefore, the selected system for this study was an IL cluster composed of 6 ion pairs confined inside a C540 cage (6_CH_BE@C540), with the objective of check the suitability of isolating small IL clusters inside fullerene cages. The fullerene cage was selected to allow the proper fit of the IL cluster.

Therefore, the main goal is this work is the study of the energetic, structural and dynamic properties of 6_CH_BE@C540 in comparison with the pristine C540Properties of CH_BE@C540 and C540 were studied in vacuum and considering CH_BE as surrounded solvent. Besides, considering the recent results by Xu et al.[19] on the electrical-driven transport of endohedral fullerenes encapsulating water molecules, the behaviour of 6_CH_BE@C540 (in vacuum and when surrounded by CH_BE solvent) under external electric fields (EEFs) was also analyzed as a function of EEF intensity. To our knowledge, this wourd would be the

first available study on endohedral fullerenes with confined ionic liquids published in open literature.

2. Computational details

2.1 Molecular Dynamics Simulations. Ionic liquids were modeled according to a forcefield parameterization previously reported,[36] whereas parameters for C540 were also previously considered.[39] Classical molecular dynamics simulations were carried out using the MDynaMix v.5.0 molecular modelling package.[47] Six CH_BE ion pairs were extracted from the central region of a cubic simulation box containing 200 ion pairs, which was simulated in the NPT ensamble at 0.1 MPa and 303 K for 5 ns, and were placed inside a C540 cage to form the endohedral fullerene. The studied systems together with the labelling used are reported in Table 1. Simulations considering one C540 cage, both for empty (pristine) and filled with 6 ion pairs, for comparison purposes, were carried out. Initial boxes for systems containing one C540 cage in CH_BE were built from rectangular boxes of $41\times41\times41$ Å^3 size, in which C540 was initially placed in a central spherical hole with radius 3 Å larger than the outer radius of C540 cage.

Molecular dynamics simulations for all the studied systems were performed at 303 K in the NVT ensemble, for the boxes size reported in the previous paragraph, with the temperature controlled using the Nose–Hoover thermostat. Coulombic interactions were handled with the Ewald summation method,[48] with cut-off radius of 15 Å. Tuckerman–Berne double time step algorithm,[49] with long and short time steps of 1 and 0.1 fs, was considered for solving the equations of motion. Lorentz-Berthelot mixing rules were used for Lennard-Jones terms. Simulations extending to 10 ns were performed.

Simulations under EEFs were done for static fields applied in the *z*-direction with 0.02, 0.04, 0.06, 0.08 and 0.10 V×Å^{-1} intensities. These non-equilibrium simulations were also done using Nose-Hoover Kinetic thermostat. The use of kinetic thermostats for non-equilibrium simulations may lead to problems because of the EEF induced drift motion contributing to the total kinetic energy, which is not separated by the thermostat from purely thermal effects, and thus, leading to an overestimation of the kinetic energy. Nevertheless, the contribution of the drift motion is strongly dependent on the intensity of the applied field; results previously reported by our group showed that in the case of CH_BE, this contribution is almost negligible for fields lower than 0.10 V×Å^{-1}.[50] Therefore the use of kinetic thermostats for the studied systems should lead to reliable results, which is in agreement with

literature available simulations of ILs under moderate EEFs.[51,52,53,54] Likewise, kinetic thermostat were also used for the simulation on EHFs under EEFs.[19]

2.2 DFT Calculations. Due to the large size of systems under study (C540, 6_CH_BE and 6_CH_BE@C540 have 540, 210 and 750 atoms, respectively), only single point calculations over structures obtained from 10 ns long molecular dynamic simulations were carried out. Moreover aimed to reduce compoutational cost, DFT calculations were carried out using a pure functional such us Perdew-Burke-Ernzerhof parameterized generalized gradient approximation (PBE)[55]. Firstly, we studied the effect of the confined IL on the electronic structure of the cage. To do this, band structure (BS) diagrams and Density of States (DOS) of pristine C540 and 6_CH_BE@C540 systems were computed considering an fcc unit cell along a set of symmetry lines within the Brilluoin zone. Partial Density of States (PDOS) was obtained using the program developed by A. Postnikov.[56] These DFT calculations were done SIESTA 3.1 code,[57] usingPBE functional along double-ζ polarized (DZP) basis set and the norm-conserving Troullier–Martins pseudopotentials.[58] Before to compute BS, lattice constant parameter for the fcc C540 crystal was estimated by assessing the minimum of the total energy as a function of the lattice constant.[59,60]

Secondly, Gaussian 09 (Revision D.01) package[61] was used to compute the binding energy and study the interaction network of the confined CH_BE cluster. Such calculations were carried out at PBE/6-31G* theoretical level. Interactions between different molecules forming the confined IL cluster were analyzed by means of Atoms in Molecules (AIM)[62 and] Natural Bond Orbital (NBO)[63] theories. Interacting molecules were localized analyzing NBO charge transfers between different units. Previously, the effect of C540 cage on intermolecular interactions between ions was checked. Firstly, this analysis was done taking into account C540 cage. Then, NBO calculations were done for the 6_CH_BE cluster, with cluster geometry obtained upon confinement in C540, but C540 surrounding cage was not considered. After comparing both analyses, our calculations showed that the surrounding cage leads to negligible effects on the charge transfer interactions between confined molecules. Therefore for the sake of simplicity, C540 cage was not considered in NBO and AIM studies. Then, we carried a topological analysis of the electronic density over different interacting ion pairs using AIM2000 program.[64]

3. Results and discussion

The studied systems, Table 1, led the analysis of several relevant issues: *i*) changes in the C540 geometrical structure and properties upon encaging IL molecules and because of IL solvation; *ii*) the structure and properties of confined IL molecules, *iii*) the characteristics of the C540 external solvation sphere, and *iv*) the behaviour of endohedral C540 fullerenes under external electric fields. Therefore, the results reported in this work are analysed and discussed separately according to abovementioned issues.

3.1 Properties of C540 molecules upon IL encaging and solvation. Molecular dynamics simulations of the systems reported in Table 1 were done considering C540 molecules as not-rigid, and thus, encaging IL pairs and surrounding the fullerene with IL should lead to changes in C540 structure in comparison with empty and isolated C540, which are analysed in this section. The calculated average C-C bond distance, $d_{C\text{-}C}$, in C540 is reported in Table 2. Dunlap and Zope[65] reported $d_{C\text{-}C}$ = 1.4264 Å obtained from quantum chemistry calculations of empty and isolated C540, this value is 2.7 % than the one reported in Table 1 for the same system, although considering the different computational approach, values reported in Table 1 may be considered as reasonable. Results reported in Table 2 show that neither confining CH_BE molecules inside C540 nor surrounding it with the IL lead to remarkable changes in $d_{C\text{-}C}$ from no IL case to IL case in/out of the C540 structure. In Table 2, the average C540 radius, R_{C540}, is also reported, which is defined as the average distance between the C540 center-of-mass and the C atoms in C540. The R_{C540} value for empty and isolated fullerene reported in Table 2 (10.7399 Å) is larger than the ones reported by Dunlap and Zoe (10.5528 Å)[65] and Ito et al. (10.53 Å),[66] obtained through quantum chemistry and tight-binding methods, respectively. R_{C540} also suffers almost negligible changes upon confining IL molecules and after solvation with IL, leading to shrinkage percentage of roughly 0.15%. These results seems to point that C540 remains almost unchanged with CH_BE inside or outside its structure, nevertheless, we have calculated radial distribution functions, $g(r)$, between the center-of-mass of the C540 and the C540 carbon atoms to quantify the structural properties, Figure 2. Results for empty fullerene in vacuum (1×PRIST_C540_VAC) show the appearance of four peaks in $g(r)$, Figure 2a; the structure around one of the twelve pentagonal sites is reported in Figures 2c and 2d, showing those atoms corresponding to the peaks in Figure 2a. Encaging CH_BE in C540 (1×6_CH_BE@C540_VAC) leads to a small weakening in the $g(r)$ peaks corresponding to atoms closer to C atoms in pentagonal sites (yellow and gray dots in Figures 2a, 2c and 2d), but the position of the maxima for the

remaining C do not change. The solvation of C540 (both empty and endohedral) leads to remarkable changes in $g(r)$, Figure 2a, peaks corresponding to C atoms close to pentagonal site vanish and only two peaks in $g(r)$ are obtained, showing that although $d_{C\text{-}C}$ and R_{C540} do not change upon IL solvation, the structure of the cage suffer subtle changes in the vicinity of the pentagonal sites. This is also confirmed by the corresponding running integrals reported in Figure 2b. Planarity around the pentagonal sites, ϕ, is defined as $\phi = 360 - (\theta_1 + \theta_2 + \theta_3)$,[66] being θ_i the angles formed by the three bonds between the C pentagonal atoms and its three nearest neighbors. Values reported in Table 2 for ϕ are larger than those reported by Ito et al.[66] for empty and isolated C540 (9.92º). The subtle changes in C540 structure inferred from $g(r)$ values in Figure 2 may be justified considering the changes in ϕ showed in Table 2, both encaging CH_BE molecules inside C540 and solvating the fullerene with CH_BE decrease ϕ for the pentagonal sites, and thus, increase planarity for those sites (ϕ = 0º would point to a fully planar site), which could justify the vanishing maxima in $g(r)$ reported in Figure 2 for those sites marked with yellow and gray symbols in the vicinity of the pentagonal carbons.

The energetics of C540 fullerene upon CH_BE confinement and solvation is reported in Table 2, in which intramolecular Lennard-Jones energy for C540, E_{intra}(LJ,C540), is reported for the studied systems. Reported results show that encaging CH_BE molecules leads to an increment in E_{intra}(LJ,C540) of roughly 0.5 eV (~ 0.5 %), both for C540 in vacuum and surrounded by IL, whereas solvation of C540 with CH_BE molecules increments E_{intra}(LJ,C540) in roughly 0.93 eV (~ 1 %), both for pristine and endohedral C540. These results are in agreement with the increasing planarity around the pentagonal sites in C540 both upon CH_BE encaging and solvation.

3.2 Properties of CH_BE confined in C540. The properties of CH_BE ions confined inside C540 fullerene should change in comparison with those ions in the bulk liquid CH_BE. Radial distribution functions between the center of mass of C540 fullerene and those for ions confined inside C540 are reported in Figure 3, for the systems in which the endohedral fullerene is in vacuum and when it is solvated by CH_BE ions. Figure 3 show that the structure of confined ions varies on going from 1×6_CH_BE@C540_VAC to 1×6_CH_BE@C540_IL, and thus, the IL molecules in the external C540 solvation shell also affect the structure of confined ions, especially for CH cation, whereas the effect on BE anion is weaker. Three peaks in $g(r)$ for CH are inferred (with maxima at 2.9, 5.7 and 6.5 Å) when endohedral C540 is in vacuum, whereas a single peak at 6.5 Å is obtained when solvated by the IL. On the contrary, for BE, although some subtle changes in $g(r)$ appear on going from vacuum to IL solvation, a well-defined peak at roughly 7.5 Å is obtained. Therefore, solvating

CH_BE@C540 endohedral fullerene with CH_BE moves CH ions from the inner spaces of the C540 toward the C540 surface. Likewise, BE ions remains 1 Å closer to the C540 carbon atoms than CH ones, which is clearly inferred from the behaviour of the running integrals reported in Figure 3b. Site-site radial distribution functions between ions selected atoms and carbon atoms in C540 are reported in Figure 4 for the 1×6_CH_BE@C540_IL system. In the case of confined BE anions, a strong peak close to C540 inner surface is obtained whereas head COO groups are placed in inner layers roughly 2 Å further of C540 inner surface. For CH cations, hydroxyl oxygen is placed in inner regions than nitrogen atoms. Once defined the radial arrangement of confined ions, the ion orientation and the spatial configuration is also inferred from molecular dynamics simulations. Results reported in Figure 5, show that BE ions stay closer to the C540 inner surface (roughly at 3.2 Å, Figure 3) than CH cations, with the anion aromatic cycles almost parallel to the C540 surface (although slightly skewed as inferred from Figure 4 results) because of π-π stacking disrupted by the curvature of the C540 inner surface. Likewise, spatial distribution functions reported in Figure 5b, show alternating layers of anion and cations with caps corresponding to BE anions in the vicinity of C540 surface, whereas CH cations occupy empty spaces rising from the arrangement of BE anions to interact with C540 π-system. To characterize the structuring of confined ions, several vectors were defined both for BE and CH, and the angles between them were used to quantify the spatial orientation with regard to C540 surface, Figure 6. For BE anion φ_1 and φ_2 angles should tend to 90º for a perfect parallel orientation of BE aromatic cycle with regard to C540 surface, results reported in Figure 6a and 6b show slight deviation from this 90º reference value, but the obtained preferential orientation would allow efficient π-π stacking with the fullerene. In the case of CH cation, results reported in Figures 6b show that cation is skewed with hydroxyl group pointing toward the interior of the C540, which is in agreement with $g(r)$ reported in Figure 4.

Energetics of endohedral systems was also analysed from molecular dynamics simulations. Intermolecular Lennard-Jones energy, E_{inter}(LJ), between the ions and C540 atoms was calculated for the 1×6_CH_BE@C540_VAC and 1×6_CH_BE@C540_IL, to infer the effects of external solvation shell ions on confined ones. E_{inter}(LJ) between confined ions and C540 atoms changes for BE from -3.61 ± 0.01 eV to -4.92± 0.01 eV, and for CH from -2.80 ± 0.01 eV to -3.28± 0.01 eV, on going from 1×6_CH_BE@C540_VAC to 1×6_CH_BE@C540_IL. Therefore, it may be concluded that BE-C540 interaction is remarkably stronger than CH-C540 one, both when the endohedral fullerene is in vacuum or surrounded by IL. Likewise, the external solvation of the endohedral fullerene with IL leads

to an improvement of the interaction between the confined ions and the internal fullerene surface, most remarkably for BE ions (increasing Lennard-Jones interaction 1.31 eV) but also for CH cations (increasing 0.48 eV), which is in agreement with the structural changes reported in the previous sections.

Effects of host-guest interactions upon ions confinement inside C540 have been also studied thoroughly analysing the changes on the electronic structure of the 1×6_CH_BE@C540_VAC system using Density Functional Theory methods for complementing the information inferred from molecular dynamics simulations in previous sections. In a first step, lattice constant parameter for C540 has been optimized, the minimal energy as a function of lattice constant was found for a value of 35.20 Å (Figure 7). There is no comparison data that is obtained experimentally for lattice constant.

Band diagrams structure for C540 and 1×6_CH_BE@C540_VAC along the symmetry directions of the fcc cubic Brilluoin zone is plotted in Figure 8. At the Γ point, a change in the energy gap is inferred, which is increased roughly 0.3eV due to the confined ionic liquid. Although the lowest unoccupied level (LUMO) practically remains constant, the highest occupied orbital (HOMO) is stabilized by 0.28 eV, whereas the Fermi level (E_F) suffers destabilization of 0.37 eV. Such increase in the E_F level leads to the lowest unoccupied levels cross with Fermi level. Unoccupied levels whose energy is slower than E_F are rather staring along all directions of the Brillouin zone, suggesting long-range interactions between the guest and the C540 cage.[60] Six unoccupied states whose energies are lower E_F were found. One of each band would be related with those levels from the cations, which have lost one electron. Changes in the BS diagram have been analyzed with the help of partial density of states (PDOS). Due to the π-electronic structure of C540, the guest PDOS were obtained considering only the contribution of p-orbitals of the atoms (see Figure 9). As expected, in the case of C540 cage, total DOS and p-orbital PDOS show a very similar behaviour. For the host-guest system, PDOS due to the atoms of the confined liquid have also calculated. Both total DOS and p-orbital PDOS show very similar profiles that are indicative that band structure is mainly due to the C540 cage. IL confined cluster atoms show slight contributions to the total DOS. On the contrary, both HOMO and LUMO levels show an important contribution from the anions oxygen atoms. Energy stabilization of the HOMO states could be related with the allocation of the anion negative charge.

A binding energy value of -14.01 eV has been estimated for the confined IL cluster and C540 cage at PBE-D/6-31G* level. Up to our knowledge, binding energies for ILs confined in fullerenes are absent of the literature. However, this large binding energy value is

indicative of energetically favoured confinement process for CH_BE IL. The interaction network of ions confined in C540 has been studied through NBO and AIM theories. In the context of AIM theory, the localization of the critical points (CP) is a very suitable tool for the characterization of the intermolecular interactions. Although there are four types of critical points, only bond critical points (BCP) were considered to analyze intermolecular interactions of confined ions. BCPs are characterized through the charge density (ρ), its Laplacian ($\nabla^2\rho$), and the ellipticity (ε), defined as $|(\lambda_1/\lambda_2) - 1|$, wherein λ_i is the largest / smallest (i=1 / i=2) curvature of the charge density in a direction perpendicular to the bond path, respectively. Ellipticity could be used to measure the extent to which charge is preferentially accumulated, and it provides a criterion for structural stability. Thus, large ellipticity values are related with weak bonds. NBO and AIM parameters for those intermolecular interactions that satisfy AIM parameters to be considered intermolecular interactions are reported in Table S1 (Supporting Information), being plotted in Figure 10. Almost all the inferred intermolecular interactions rise from the lone pair of both oxygen atoms in the anion acting as donors and hydrogen atom in the cation acting as acceptors. Only NBO charge transferences whose values are larger than 0.05 eV satisfy AIM criteria. As noted in Figure 10, confined IL cluster adopts a spherical configuration. As expected, the largest NBO charge transfer correspond with large ρ and small ε, and also with the shortest donor – acceptor distances. Besides, the strongest interactions are those wherein the phenyl motif of the benzoate anion tends to be parallel to the C540 aromatic rings, with a typical π-π stacking distance, being indicative of a π-stacking interaction.

NBO charge distribution for the confined IL molecules has been also analysed, Table 3. All equivalent atoms show similar charge values, independently of their position in the confined cluster. According with the molecular structure of the cation, positive charge should be allocated over N atoms, which yield a charge of -0.29 a.u. The calculated total charge of the cation is 1.16 a.u. On the other hand, negative charge in the anion should be allocated over both O atoms, which show a charge of -0.73 a.u., with the total anion charge being - 0.85 a.u. This effect is related with a charge transfer of around 0.3 eV between the cation and the anion. This charge transfer energy is very similar to the change in the HOMO state due to the confined IL. Then, a relationship between stabilization of the HOMO state and charge transfer between IL ions could be established.

HOMO and LUMO states for 1×6_CH_BE@C540_VAC system also show an important contribution from the confined IL cluster, Figure 11. As expected from PDOS results, HOMO and LUMO orbitals are mainly located on anions. LUMO orbitals, are mainly

delocalized over all the anion, whereas HOMO is mainly located over COO- motifs. Although Figure 11 only plots the HOMO and LUMO orbital, an analogous behaviour was inferred for the six orbitals below and above.

3.3 Properties of C540 external solvation by CH_BE. The analysis of the effect of external solvation shells on the properties of ions confined inside C540 fullerene was carried out in previous section, on the following, the structuring of CH_BE ions externally solvating C540 fullerene will be analysed. Figure 12 shows $g(r)$ for the systems formed by 1 C540 fullerene surrounded by the ionic liquid, both in the cases of empty (1×PRIST_C540_IL, Figure 12a) and filled with IL (1×6_CH_BE@C540_IL, Figure 12b) fullerene. $g(r)$ for BE and CH ions show strong peaks for the first external solvation shell, both for empty and endohedral C540. BE anions are roughly 1 Å closer to the C540 external surface than CH anions, in parallel with the behaviour of confined ions with regard to the internal C540 surface, Figure 12b. The distance between the center of mass for externally solvating BE anions and the C540 surface is 3.2 Å, whereas it is 4.2 Å in the case of CH cations, for 1×PRIST_C540_IL. The external solvation of the fullerene by the IL is weakly affected by the presence of confined ions inside the C540 (1×6_CH_BE@C540_IL); nevertheless, results reported in Figure 12 show that confining CH_BE ions inside C540 leads to and approaching of the first CH_BE external solvation shell to the C540 surface by roughly 0.1 Å, which is in agreement with effect of the external shell on internal confined ions. Site-site $g(r)$ between C540 carbon atoms and selected ion sites for externally solvating ions are reported in Figure 13 for empty and endohedral C540. A comparison between results reported in Figures 4 and 13 show similar structuring on the C540 surface both for CH_BE ions inside and outside of the fullerene. Likewise, the effect of confined ions on the structuring of the external ionic solvation shell is very weak, as it may be inferred from the comparison of Figures 13a and 13b; nevertheless, to quantify this effect, the differences between the running integrals obtained from $g(r)$ for the solvation of empty and endohedral C540 are reported in Figure 14. The first external solvation shell (r~<10 Å) is slightly richer in BE ions for empty fullerene than for endohedral one, whereas the opposite effect is obtained for CH cation. Spatial arrangement around C540 for ions externally solvating the fullerene are reported in Figure 15. The snapshot showed in Figure 15a probes BE ions lying almost parallel to the C540 external surface, with a slight skew in agreement with $g(r)$ reported in Figure 13. Spatial distribution function reported in Figure 15b show alternating layers of anions and cations, with BE anions closer to the C540 surface and CH cations occupying the available space. Ions orientations in the external shell is also analysed through the order parameters defined for the molecular vectors reported in

Figure 16, showing a strong preferential orientation for CH and BE ions, with parallel almost arrangements of both ions in the first external shell.

The energetics for the interaction between the externally solvating ions and C540 is reported in Table 4. Reported results show stronger BE-C540 than CH-C540 interactions (roughly 2 eV stronger), which may be justified considering that BE anions are closer to the C540 external surface than CH cations, as reported in previous sections. Moreover, putting C540 inside the IL weakens CH-BE interactions, both for coulombic and Lennard-Jones contributions, in comparison with those in pure CH_IL (with no C540).[67] Nevertheless, this decrease in anion-cation interaction strength upon C540 solvation evolves in parallel with a decrease in anion-anion and cation-cation coulombic repulsive energies. Therefore, the total balance of interionic energy, defined as the difference between anion-cation interaction energy minus the sum of anion-anion and cation-cation contributions, is -5.49 eV for pure CH_BE whereas it is -5.79 and -5.56 eV, for 1×PRIST_C540_IL and 1×6_CH_BE@C540_IL, respectively. Likewise, the total ion-C540 interactions are -19.19 and -27.39 eV, for 1×PRIST_C540_IL and 1×6_CH_BE@C540_IL, respectively. Therefore, placing C540 fullerene into CH_BE is strongly energetically favoured.

The dynamic properties of the studied endohedral fullerene are of importance to characterize the studied systems. Self-diffusion coefficients, *D*, were obtained using molecular dynamics simulations trajectories from mean square displacements and Einstein's equation. Diffusion properties for 1×6_CH_BE@C540_IL system were calculated for ions confined inside the fullerene, in the first external solvation shell (defined according to the first minima in $g(r)$ reported in Figure 12), and the remaining fluid layers, Table 5. Ions confined inside C540 fullerene show very low *D* values, being two orders of magnitude than those for bulk CH_BE in absence of fullerene, and showing a solid-like behaviour of confined ions. This slow dynamics of ionic liquids upon confinement has been also reported in carbon nanotubes,[39,68] , and it may be explained considered the formation of a crystal-like phase of ions when confined inside of carbon nanostructures.[69] Nevertheless, this effect is strongly dependent on the size of ions and the width of the carbon nanotube, Ohba and Chaban[70] have recently reported that for 1-ethyl-3-methylimidazolium chloride confinement in (10,10) carbon nanotubes leads to an increase of 1.5 orders of magnitude for the diffusion rates in comparison with the bulk fluid, whereas in the case of (22,22) carbon nanotube diffusion rates are similar or slightly lower to that in bulk fluid, depending on the temperature. This behaviour is justified considering the disruption of the ionic liquid network upon confinement, and thus. Nanotubes with large diameter are able to maintain the most relevant

features of the bulk fluid when ions are confined. In the case of confinement in large fullerenes, when the cage is fully filled with ions as it is done in this work, the mobility of the ions is very low and anion-cation intermoleculecular forces are very strong, which would justify the poor diffusion rates obtained from molecular dynamics simulations.

Likewise, ions in the first external solvation shell also show very low *D* values, even lower than those confined, which may be justified considering the strong interaction with the C540 surface as inferred from the energetics reported in Table 4. *D* values for BE anions confined and in the first external solvation shell are lower than those for CH cations, which is in contrast with the behaviour of more external ions or in the bulk CH_BE. This may be justified considering the stronger BE-C540 interaction in comparison with CH-C540, because of the π-π stacking of BE ions. Banerjee[71] reported a study on the solvation of fullerenes by water, toluene and acetone, in which showed that molecules in the first external solvation shell had reduced mobility in comparison with bulk molecules. For example, results from Banerjee et al.[71] in water – C540 system, showed *D* values of 2.1 and 2.4×10^{-9} m^2 s^{-1} for water molecules in the first solvation shell and in bulk phase, respectively. Viscosity of CH_BE IL is three orders of magnitude larger than that of water, and so are the self-diffusion coefficients, but additionally to this effect, water molecules decreases their mobility roughly a 12 % on going from bulk water to C540 solvation layer, whereas e.g. the mobility of BE ions is 60-times lower in the solvation layer than in the bulk IL. Banerjee et al.[71] also reported studies on toluene-C60 showing that toluene mobility decreases a 25 % on going to fullerene solvation shells, which is almost the double effect than for water molecules, and thus, showing the importance of the π-π interaction with the fullerene. Nevertheless, changes in ionic mobility on ILs going to fullerene solvation shells are remarkably larger than those for organic solvents. The diffusion of CH_BE ions placed further of the first C540 external solvation shell approaches that of pure CH_BE, although *D* values are lower for 1×6_CH_BE@C540_IL than for pure CH_BE, and thus, showing that the disrupting effect of C540 on IL structure extends to large distances of the fullerene, in agreement with the behaviour of $g(r)$ showed in Figure 12. Likewise, the self-diffusion coefficient of C540 in CH_BE was also calculated leading to $(0.0004\pm0.0002)\times10^{-11}$ m^2 s^{-1}, this very low *D* value should be considered with caution because of the length of the simulations (obviously fully diffusive regime was not reached for C540 in the applied simulation time), but it shows, at least qualitatively the low mobility of the studied giant fullerene in CH_BE.

3.4 Endohedral fullerenes under external electric fields. In a recent work, Xu and Chen proposed to control direction and rate of transport of endohedral C60 fullerenes containing a

single water molecule using external electric fields,[19] and thus, encouraged by their results, the behaviour of 1×6_CH_BE@C540_IL under EEFs was studied as a way to control the slow diffusion of the studied C540 endohedral fullerene in CH_BE. For comparative purposes, the behaviour of an empty C540 fullerene, 1×PRIST_C540_IL, under EEFs was also studied. In a recent work,[72] our group reported a study on the behaviour of bulk CH_BE (among other ILs) under EEFs. These previous results showed that CH_BE has an intrinsic electric field of 0.36 V×Å^{-1} and 0.31 V×Å^{-1}, for BE and CH ions, respectively. Therefore, considering that EEFs applied in this work were lower than 0.10 V×Å^{-1}, the effect of EEFs on the studied systems should be moderate. Nevertheless, the possible application of stronger EEFs was discarded considering the common range of applied fields for technical applications. The molecular dynamics simulations carried out in this work under EEFs were done using fields applied along the z-direction, and thus, the z-component of the total dipole moment, μ_Z, was calculated for the studied systems. Figure 17 shows μ_Z values for BE anions under EEFs for the first ns of simulations, and for ions confined inside the fullerene, in the first external shell and in outer regions. Results in Figure 17a show that ions confined inside C540 are not affected by the applied EEFs (for $E \leq 0.10$ V×Å^{-1}), and thus, the fullerene acts as a screening cage of the confined ions. These results may seem puzzling, Amusia and Bantelkov[73] showed that C60 fullerene under a static electric field behaves as a set of separate atoms instead of a conducting sphere, and thus, the fullerene cage would not be able to fully screen the external electric field. Nevertheless, Connerade et al.[74] and Lo et al.[75] analyzed the dynamical screening of fullerenes and showed that in the static limit confined atoms are completely shielded from the external field; moreover, this screening effect against electromagnetic radiation stands for frequencies lower than 20 eV. Therefore, in the case of the endohedral systems studied in this work (ionic liquid@C540), we have to consider several factors that justify the strong screening of the C540 cage: *i*) the studied ionic liquids have a strong intrinsic electric field, as aforementioned, *ii*) the applied external fields are lower than 0.10 V×Å^{-1}, *iii*) the strong ion-C540 interactions, because cage is fully filled with ions instead of placing a single molecule inside of it.

For ions solvating C540 in the first layer, Figure 17b, the reported results also show almost negligible effect of the applied fields, which is in agreement with the strength of the ions-C540 interactions reported in previous sections. Ions in regions further of the first C540 shell, are only affected by the field for the stronger cases studied. Analogous results were inferred for CH cation and for the behaviour of empty fullerene under EEFs.

4. Conclusions

A combined DFT and molecular modelling study of the properties of Choline benzonate ionic liquid encapsulated in endohedral C540 fullerene is reported in this work. The behaviour of ions confined inside the fullerene is characterized by the strong π- π stacking of BE anions on C540 walls, which determine the structure of the confined ion pairs, with CH cations occupying the available empty spaces in more internal regions, but also being able of interact with the fullerene. The structure of the confined ions is affected by the presence or absence of ions solvating externally the C540, which seem to improve the ion-C540 interactions for confined ions. DFT studies on the electronic properties of CH_BE@C540 fullerene show changes on the band structures and density of states of C540 upon ions confinement, which rise from the ions-C540 interactions, which are characterized by AIM and NBO analysis. The results from the application of EEFs for the studied endohedral fullerenes show that C540 acts as a perfect Faraday cage for the confined ions, but the very strong interaction between the ions in the first external C540 solvation layer and C540 surface also leads to almost negligible effects of applied EEFs on these ions. Only when large EEFs are applied, some effects are obtained on the structuring of ions in regions further of the first solvation layers of C540.

More generally, theoretical simulations carried out in this work could be used both in the prediction of the properties and the rational design of of new materials based on IL cluster confined in fullerenes for technological applications.

ACKNOWLEDGEMENTS

Gregorio García acknowledges the funding by Junta de Castilla y León, cofunding by European Social Fund, for a postdoctoral contract. We also acknowledge the Computing and Advanced Technologies Foundation of Extremadura (CénitS, LUSITANIA Supercomputer, Spain) and the Foundation of Supercomputing Center of Castile and León (FCSCL, CALÉNDULA Supercomputer, Spain) for providing supercomputing facilities. The statements made herein are solely the responsibility of the authors.

Electronic supplementary information (ESI): NBO and AIM results (Table S1). This material is available free of charge via the Internet at http://pubs.acs.org.

Table 1 Systems considered in this work for molecular dynamics simulations. *N* stands for the number of C540 fullerene cages considered in the simulation and ILpairs@C540 stands for the number of ion pairs confined inside the C540 cage

label	*N*	medium	IL pairs @C540	IL pairs outside C540
1×PRIST_C540_VAC	1	vacuum	0	0
1×PRIST_C540_IL	1	CH_BE	0	185
1×6_CH_BE@C540_VAC	1	vacuum	6	0
1×6_CH_BE@C540_IL	1	CH_BE	6	185

Table 2 Average C-C bond distance, $d_{C\text{-}C}$, for atoms in C540 fullerene, average C540 fullerene radius, R_{C540}, and average planarity, ϕ, and average intramolecular Lennard-Jones energy for C540, E_{LJ}(C540). Systems defined as in Table 1. All values obtained from molecular dynamics simulations at 303 K

system	$d_{C\text{-}C}$ / Å	R_{C540} / Å	ϕ / deg	E_{LJ}(C540) / eV atom^{-1}
1×PRIST_C540_VAC	1.4530±0.0184	10.7399±0.3804	11.04±3.23	50.92±0.00
1×PRIST_C540_IL	1.4529±0.0174	10.7311±0.3984	8.89±3.37	51.88±0.01
1×6_CH_BE@C540_VAC	1.4522±0.0173	10.7340±0.3889	9.42±2.08	51.40±0.01
1×6_CH_BE@C540_IL	1.4509±0.0180	10.7224±0.3964	8.08±4.25	52.31±0.01

Table 3 NBO charge distribution for atoms in CH_BE confined inside C540 (1□6_CH_BE@C540_VAC). See Figure 1 for atom labelling

atom	NBO charge / a. u. [a]
N1	-0.29
C1	-0.50
H_{al} [b]	0.28
C2	-0.28
C3	-0.14
O1	-0.77
H4	0.50
C6 / C7	-0.23
C5	-0.15
C4	0.72
O2	-0.73
H_{ar} [c]	0.24

[a] Reported data are average values over all the CH_BE atoms confined inside C540.
[b] Alkyl hydrogen atoms in CH cation.
[c] Aromatic hydrogen atoms in BE anion.

Table 4 Interaction energies, E_{inter}, between the reported constituents in the systems 1×PRIST_C540_IL, 1×6_CH_BE@C540_IL and in the pure ionic liquid (CH_BE, ionic liquid in absence of C540 fullerene). All values obtained from molecular dynamics simulations at 303 K. Coul and LJ stand for coulombic and van der Waals components of the total interaction energy. All values in eV

	CH_BE[a]		1×PRIST_C540_IL		1×6_CH_BE@C540_IL	
	E_{inter}(Coul)	E_{inter}(LJ)	E_{inter}(Coul)	E_{inter}(LJ)	E_{inter}(Coul)	E_{inter}(LJ)
BE─C540	–	–	–	-10.61	–	-15.53
CH─C540	–	–	–	-8.59	–	-11.87
BE─CH	-27.68	-0.38	-27.15	-0.35	-26.77	-0.34
BE─BE	11.34	-0.16	10.87	-0.16	10.78	-0.15
CH─CH	11.55	-0.15	11.15	-0.16	11.07	-0.15

[a] Values for pure CH_BE obtained at 298 K (Ref. 67).

Table 5 Center-of-mass self-diffussion coefficients, D, in the system 1×6_CH_BE@C540_IL. All values obtained from molecular dynamics simulations at 303 K. Values calculated for ions confined inside the C540 fullerene, $r < R_{C540}$, ions in the first external solvation shell of C540 fullerene, $R_{C540} < r < 17$ Å, and for ions in outer C540 fullerenes solvation shells, $r > 17$ Å, where r stands for the distance between the center of mass of C540 and the center of mass of the corresponding ion, and R_{C540} is C540 average radius reported in Table 2. The definition of solvation shells is done according radial distribution functions reported in Figure 12b

		$10^{11} \times D$ / m^2 s^{-1}	
shell	r / Å	BE	CH
CH_BE[a]	–	0.1107±0.0051	0.0983±0.0049
ions inside C540	$r < R_{C540}$	0.0024±0.0006	0.0035±0.0004
ions in the first external solvation shell of C540	$R_{C540} < r < 17$	0.0015±0.0008	0.0017±0.0008
ions in outer external solvation shell of C540	$r > 17$	0.0963±0.0039	0.0900±0.0040

[a] Values calculated for pure CH_BE in absence of C540.

Figure Captions.

Fig. 1 Molecular structure of choline, CH, and benzoate, BE, ions considered in this work.

Fig. 2 (a) Radial distribution function, $g(r)$, and (b) the corresponding running integrals of $g(r)$, N, between the center of mass of C540 and the C540 carbon atoms for the reported systems, with system labelling as in Table 1. In panels (c) and (d), carbon atoms around a pentagonal site in C540 are reported (top and side views), with atoms color code used to define those atoms corresponding to the maxima in $g(r)$ showed in panel (a). In panels (c) and (d) only pentagonal site is showed for the sake of visibility, and in panel (d) the remaining atoms of C540 are also omitted. Dashed gray vertical lines in panel (b) show the position of maxima in $g(r)$ reported in panel (a). All values obtained from molecular dynamics simulations at 303 K.

Fig. 3 (a) Radial distribution functions, $g(r)$, and (b) the corresponding running integrals, N, between the center of mass of C540 and the center of mass of CH cation and BE anion for ions confined inside C54, with system labelling as in Table 1. r = 0 Å corresponds to C540 center of mass, and the vertical gray dashed line shows the position of C540 carbon atoms, defined as the average C540 radius reported in Table 2. All values obtained from molecular dynamics simulations at 303 K. In the case of 1×6_CH_BE@C540_IL system only $g(r)$ inside the C540 is reported.

Fig. 4 Radial distribution functions, $g(r)$, between the carbon atoms in C540 (C) fullerene and selected atoms in CH and BE ions, for 1 endohedral C540 fullerene encaging 6 CH_BE ion pairs surrounded by CH_BE ionic liquid (1×6_CH_BE@C540_IL in Table 1). Atoms code as in Figure 1. All values obtained from molecular dynamics simulations at 303 K. Only ions inside the C540 fullerene are considered in the calculation of $g(r)$.

Fig. 5 (a) Representative snapshot and (b) spatial distribution function, for CH and BE ions confined inside C540, for 1 endohedral C540 fullerene encaging 6 CH_BE ion pairs surrounded by CH_BE ionic liquid (1×6_CH_BE@C540_IL in Table 1). All values obtained from molecular dynamics simulations at 303 K. Color code: (blue) CH cation and (green) BE anion. In panel (b), dashed red line show the position of C540 surface, defined with the average C540 radius reported in Table 2.

Fig. 6 Orientation of ions confined inside C540 fullerene. All values calculated for 1 endohedral C540 fullerene encaging 6 CH_BE ion pairs surrounded by CH_BE ionic liquid (1×6_CH_BE@C540_IL in Table 1). All values obtained from molecular dynamics simulations at 303 K.

Fig. 7 Energy convergence as a function of the lattice constant parameter for C540 cage.

Fig. 8 Electronic Band structure for (a) pristine C540 and (b) 6_CH-BE@C540 systems. Dotted lines represent Fermi level.

Fig. 9 Total and PDOS of (a) pristine C540 cage and (b) 6_CH-BE@C540 systems.

Fig. 10 Different views for the schematic representation of the interaction network for CH_BE confined inside the C540 cage. For clarity, C540 cage and non-interacting H atoms are omitted. C, O, N and H are represented in grey, red, blue and green respectively.

Fig. 11 Isovalues of (a) HOMO and (b) LUMO molecular orbitals for 6_CH_BE cluster confined in C540. Values calculated at PBE-D/6-31G* level.

Fig. 12 Radial distribution functions, $g(r)$, between the center of mass of C540 and the center of mass of CH cation and BE anion for (a) 1 empty C540 fullererene surrounded by CH_BE ionic liquid (1×PRIST_C540_IL in Table 1), and (b) 1 endohedral C540 fullerene encaging 6 CH_BE ion pairs surrounded by CH_BE ionic liquid (1×6_CH_BE@C540_IL in Table 1). All values obtained from molecular dynamics simulations at 303 K. r = 0 Å corresponds to C540 center of mass, and the vertical gray dashed line shows the position of C540 carbon atoms, defined as the average C540 radius reported in Table 2.

Fig. 13 Radial distribution functions, $g(r)$, between the carbon atoms in C540 (C) fullerene and selected atoms in CH and BE ions, for (a) 1 empty C540 fullererene surrounded by CH_BE ionic liquid (1×PRIST_C540_IL in Table 1), and (b) 1 endohedral C540 fullerene encaging 6 CH_BE ion pairs surrounded by CH_BE ionic liquid (1×6_CH_BE@C540_IL in Table 1). Atoms code as in Figure 1. All values obtained from molecular dynamics simulations at 303 K. In panel b, only ions outside the C540 fullerene are considered in the calculation of $g(r)$. r = 0 Å corresponds to the position of C540 carbon atoms.

Fig. 14 Running integrals, N, differences, obtained from the corresponding radial distribution functions reported in Figure 13, between values for 1 empty C540 fullererene surrounded by CH_BE ionic liquid ($N_{1\times\text{PRIST\_C540\_IL}}$, defined as in Table 1), and 1 endohedral C540 fullerene encaging 6 CH_BE ion pairs surrounded by CH_BE ionic liquid ($N_{1\times\text{6\_CH\_BE@C540\_IL}}$, defined as in Table 1). Atoms code as in Figure 1. For $N_{1\times\text{6\_CH\_BE@C540\_IL}}$ only ions outside C540 were considered, as in Figure 13.

Fig. 15 (a) Representative snapshot and (b) spatial distribution function, for CH and BE ions in the first external solvation shell of C540 for 1 endohedral C540 fullerene encaging 6 CH_BE ion pairs surrounded by CH_BE ionic liquid (1×6_CH_BE@C540_IL in Table 1). All values obtained from molecular dynamics simulations at 303 K. Color code: (blue) CH cation and (green) BE anion. In panel (b), dashed red line show the position of C540 surface, defined with the average C540 radius reported in Table 2.

Fig. 16 Orientation of ions outside C540 fullerene. All values calculated for 1 endohedral C540 fullerene encaging 6 CH_BE ion pairs surrounded by CH_BE ionic liquid (1×6_CH_BE@C540_IL in Table 1). All values obtained from molecular dynamics simulations at 303 K. Vectors defined as in Figure 6. Vertical gray dashed lines stand for the position of the first external solvation shell defined according to $g(r)$ in Figure 12.

Fig. 17 Total dipole moment along the z-direction for BE anions, μ_Z, for 1 endohedral C540 fullerene encaging 6 CH_BE ion pairs surrounded by CH_BE ionic liquid (1×6_CH_BE@C540_IL in Table 1) under EEFs. BE anions (a) confined inside C540, (b) in the first external C540 solvation shell, and (c) in outer shells.

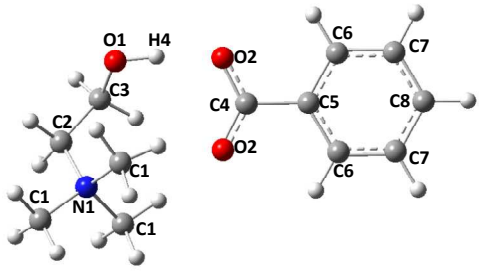

Figure 1.

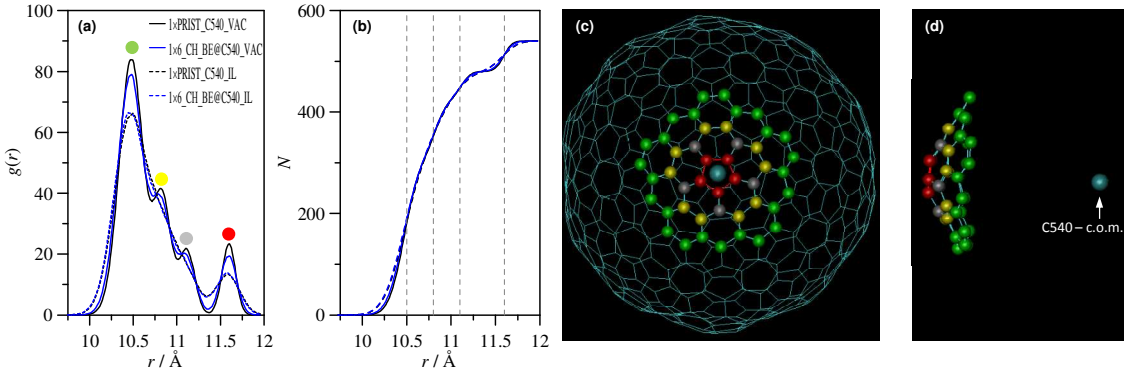

Figure 2.

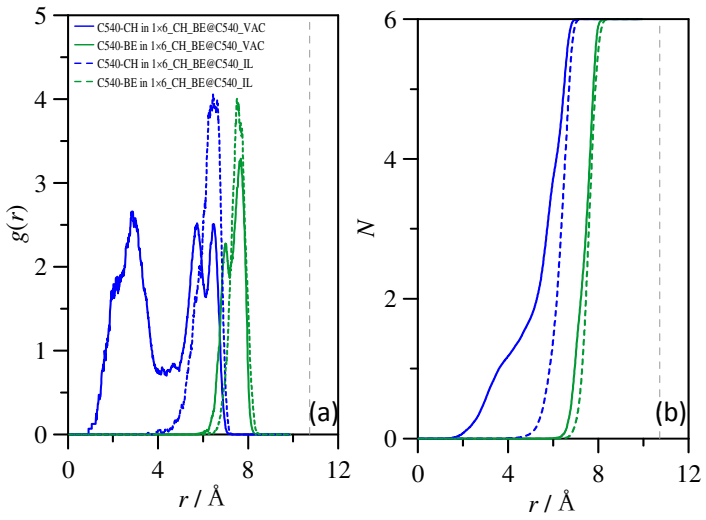

Figure 3.

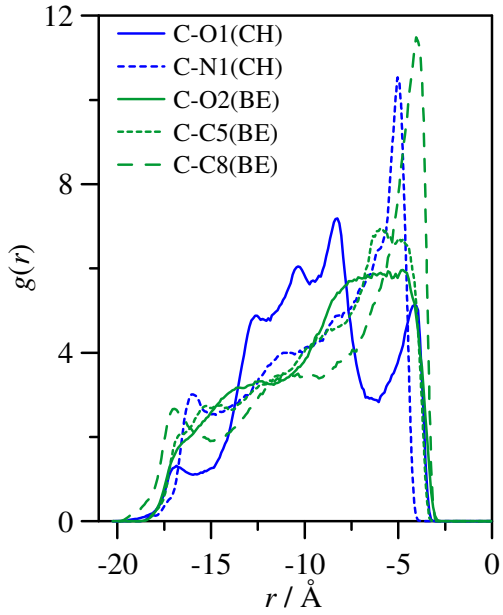

Figure 4.

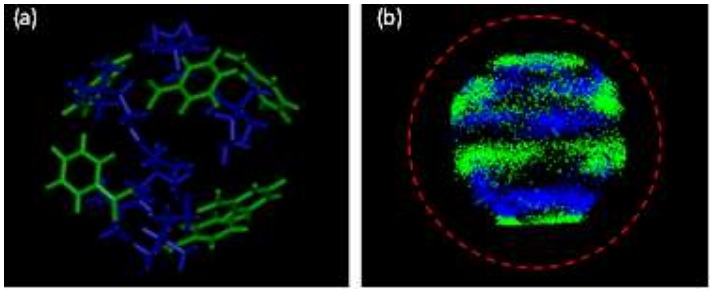

Figure 5.

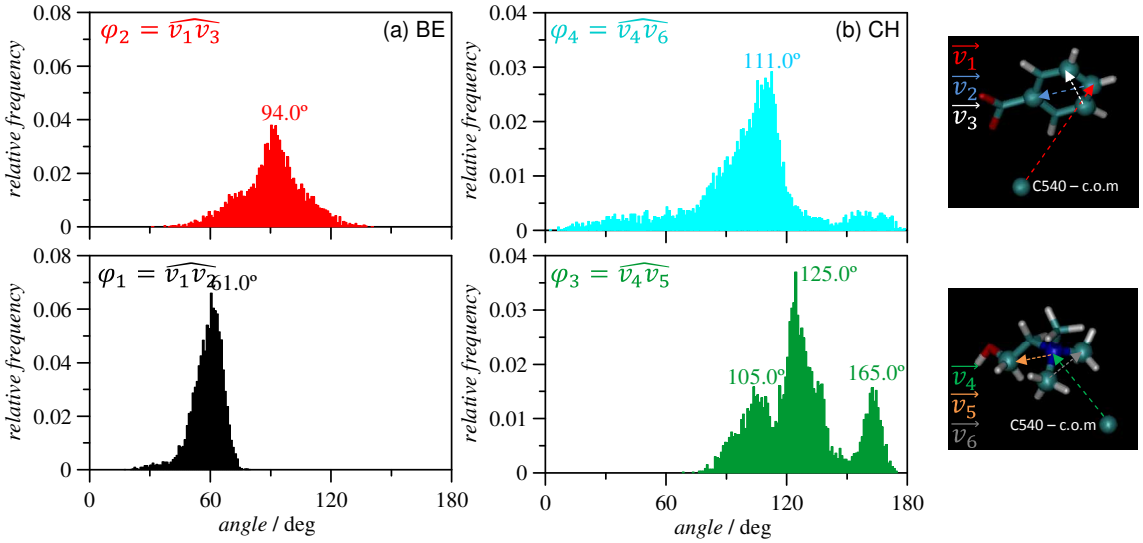

Figure 6.

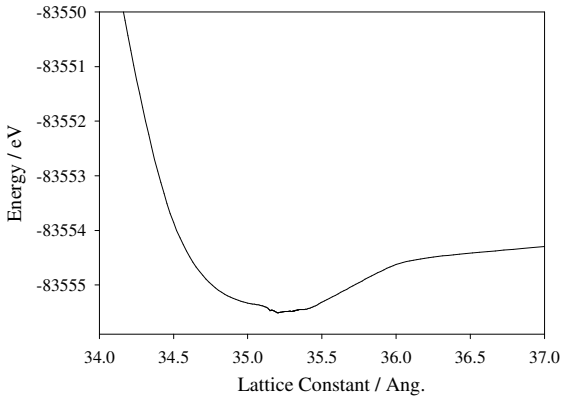

Figure 7.

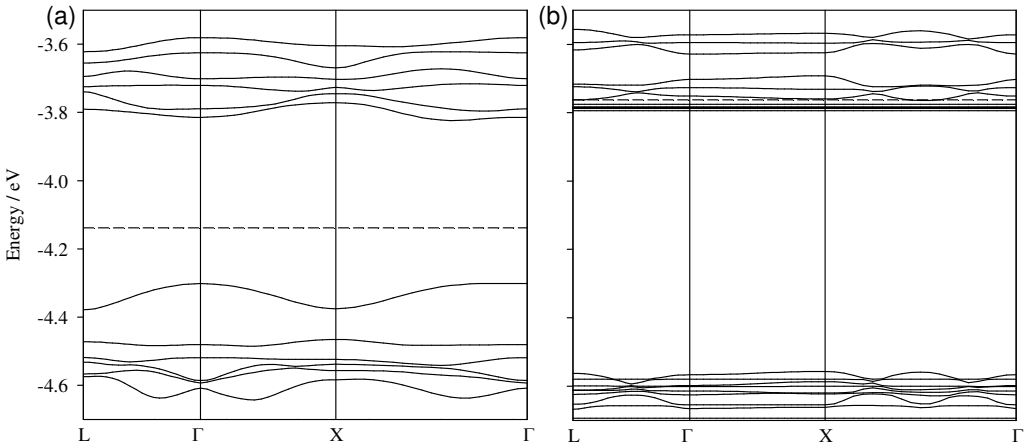

Figure 8.

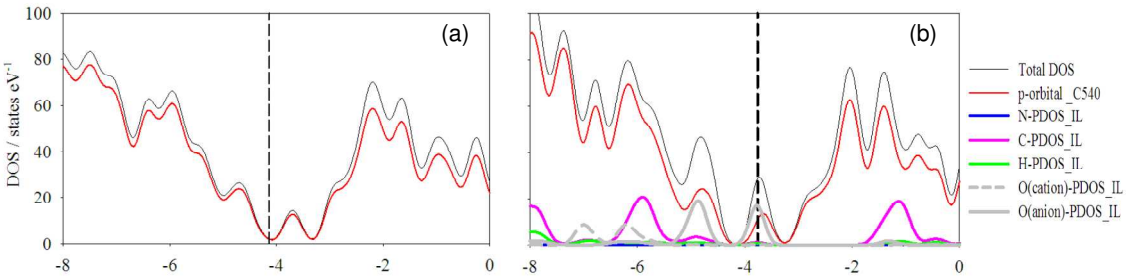

Figure 9.

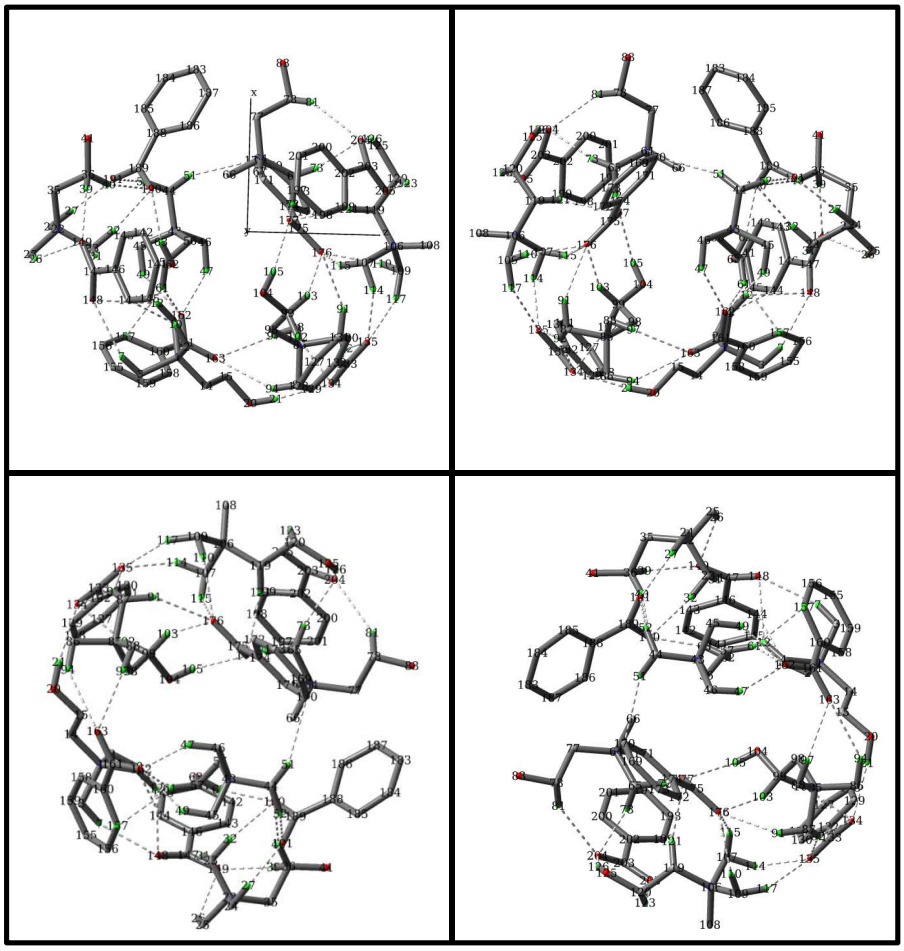

Figure 10.

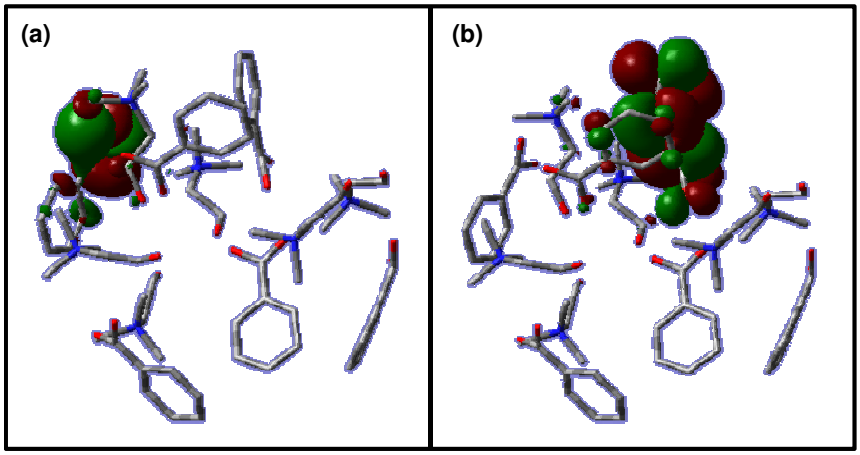

Figure 11.

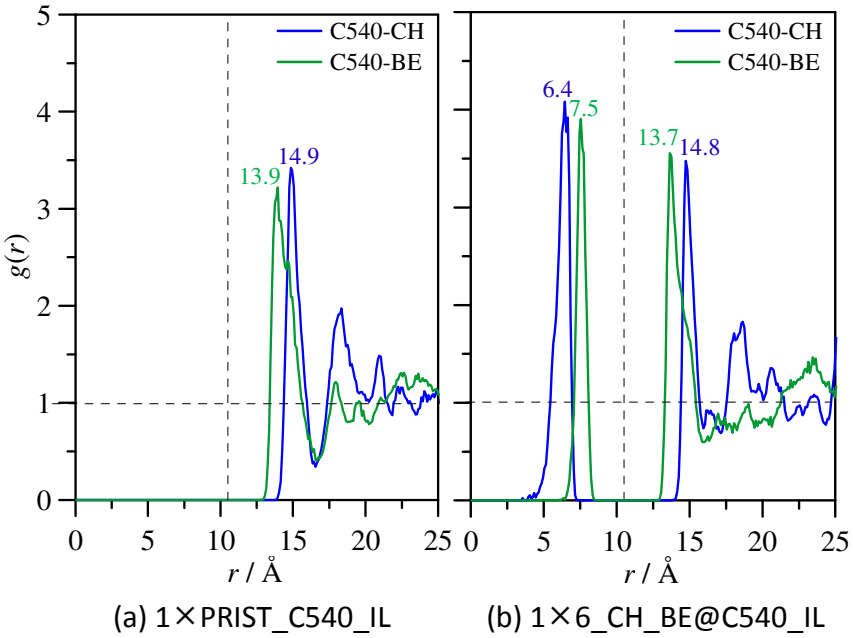

Figure 12.

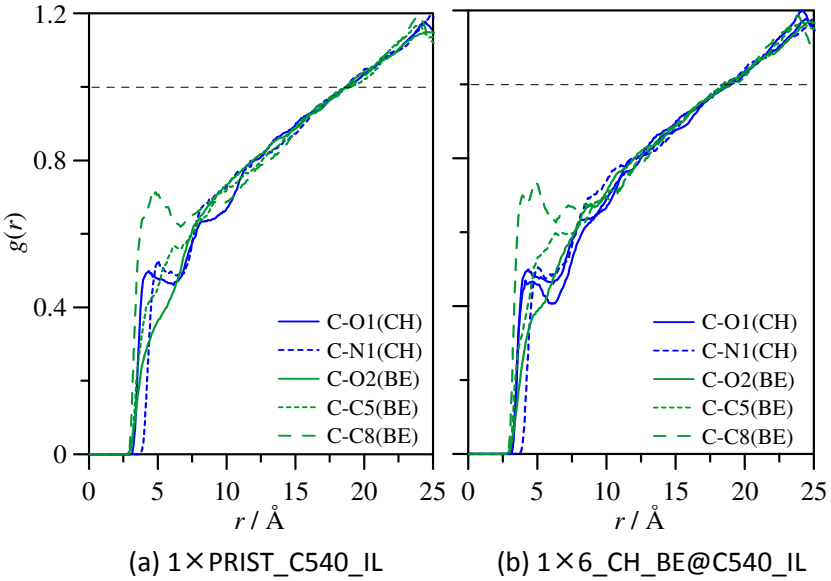

Figure 13.

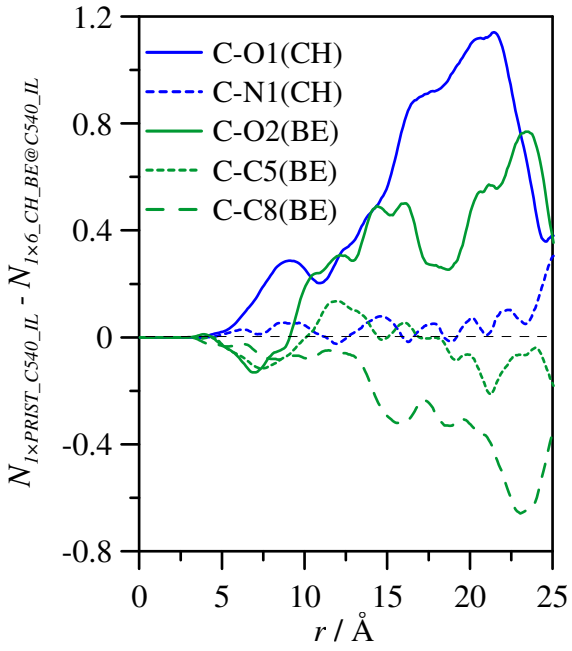

Figure 14.

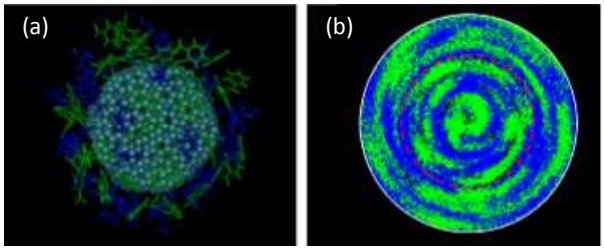

Figure 15.

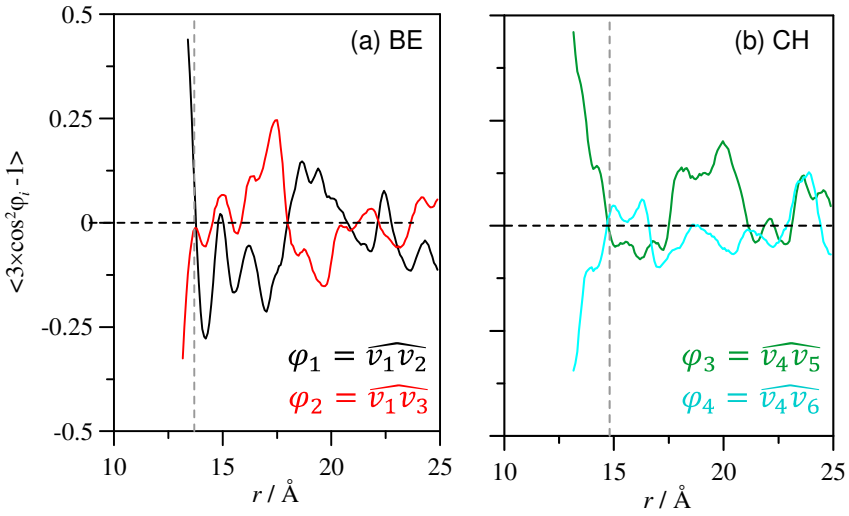

Figure 16.

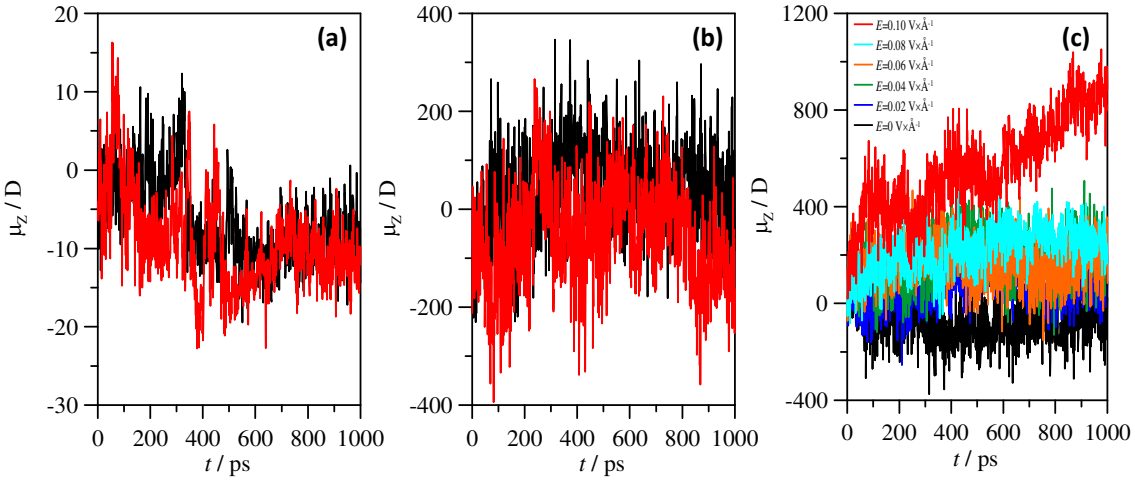

Figure 17.

References

1. H. Shinohara. *Rep. Prog. Phys.* 2000, **63**, 843-892.
2. T. Akasaka, S. Nagase, S. *Endofullerenes: A New Family of Carbon Clusters.* Kluwer: Dordretch, 2002.
3. A. A.Popov, S. Yang, L. Dunsch, L. *Chem. Rev.* 2013, **113**, 5989-6113.
4. A. Rodríguez-Fortea, A. L. Balch, J. M. Poblet. *Chem. Soc. Rev*. 2011, **40**, 3551-3563.
5. S. Osuna, M. Swart, M. Solá. *Phys. Chem. Chem. Phys*. 2011, **13**, 3585-3603.
6. D. M.Rivera-Nazario, J. R. Pinzón, S. Stevenson, L. A. Echegoyen. *J. Phys. Org. Chem.* 2013, **26**, 194-205.
7. T.Akasaka, X. Lu. *Chem. Rec.* 2011, **12**, 256-269.
8. N. J.Turro, J. Y. C. Chen, E. Sartori, M. Ruzzi, A. Marti, R. Lawler, S. Jockusch, J. López-Gejo,; K. Komatsu, Y. Murata. *Acc. Chem. Res*. 2010, **43**, 335-345.
9. M. Rudolf, S. Wolfrum, M. Guldi, L. Feng, T. Tsuchiya, T. Akasaka, L. Echegoyen. *Chem. Eur. J.* 2012, **18**, 5136-5148.
10. L. Feng, M. Rudolf, S. Wolfrum, A. Troeger, Z. Slanina, T. Akasaka, S. Nagase, N.,Martín, T. Ameri, C. Brabec, D. M. Guldi. *J. Am. Chem. Soc*. 2012, **134**, 12190-12197.
11. F P. atouros, M. D. Shultz. *Nanomedicine*. 2013, **8**, 1853-1864.
12. M. Carini, L. Dordevic, T. Da Ros, *Fullerenes in Biology and Medicine*. In: Handbook of Carbon Nanomaterials. Vol. 3: Medicinal and Bio-related Applications. D'Souza, F. Kadish, K. M. Eds.. , World Scientific, 2012, pp. 1-47.
13. R. B. Ross, C. M. Cardona, D. M. Gauldi, S. G. Sankaranarayanan, M. O. Reese, N. Kopidakis, J. Peet, B. Walker, G. C. Bazan, E. V. van Keuren, B. C. Holloway, M. Drees. *Nature Mat*. 2009, **8**, 208-212.
14. H. Dodziuk, G. Dolgonos, O. Lukin. *Carbon* 2001, **39**, 1907-1911.
15. Y. X. Ren, T. Y. Ng, K. M. Liew. *Carbon*. 2006, **44**, 397-406.
16. R. E. Barajas-Barraza, R. A.Guirado-López. *Phys. Rev. B* 2002, **66**, 155426.
17. Q. Zhang, T. Pankewitz, S. Liu, W. Klopper, L. Gan. *Angew. Chem. Int. Ed.* 2010, **49**, 9935-9938.
18. L. Shi, L. Gan. *J. Phys. Org. Chem.* 2013, **26**, 766-772.
19. B. Xu, X. Chen. *Phys. Rev. Lett.* 2013, **110**, 156103.
20. C. N. Ramachandran, N. Sathyamurthy. *Chem. Phys. Lett.* 2005, **410**, 348-351.
21. J. Hernández-Rojas, V. Monteseguro, J. Bretón, J. M. Gómez-Llorente. *Chem. Phys.* 2012, **399**, 240-244.
22. O. P. Charkin, N. M.Klimenko. *Adv. Quantum. Chem*. 2009, **58**, 69-114.
23. M. D. Ganji M. Mohseni, O.Goli. *J. Mol. Struc. Theochem*. 2009, **913**, 54-57.
24. C. A. Angell, Y. Ansari, Z.Zhao. *Faraday Discuss.* 2012, **154**, 9-27.
25. E. T. Fox, E. F. Weaver, W. A. Henderson. *J. Phys. Chem. C* 2012, **116**, 5270-5274.
26. A. T. Kurananithi, A. Mehrkesh. *AIChE J.* 2013, **59**, 4627-4640.
27. N. V. Plechkova, K. R. Seddon. *Chem. Soc. Rev.* 2008, **37**, 123-150.
28. S. Werner, M. Haumann, P.Wasserscheid. *Ann. Rev. Chem. Eng*. 2010, **1**, 203-230.
29. T. Fukushima, A. Kosaka, Y. Ishimura, T. Yamamoto, T. Takigawa, N. Ishii, T.Aida. *Science* 2003, **300**, 2072-2074.
30. T. Fukushima, T. Aida. *Chem. Eur. J.* 2007, **13**, 5048-5058.
31. M. Sha, G. Wu, Y. Liu, Z. Tang, H. Fang. *J. Phys. Chem. C* 2009, **113**, 4618-4622.
32. S. Maolin, Z. Fuchun, W. Guozhong, F. Haiping, W. Chunlei, C. Shimou, Z. Yi, H. Jun. *J. Chem. Phys.* 2008, **128**, 134504.
33. S. Wang, S. Li, Z. Cao, T. Yan. *J. Phys. Chem. C* 2010, **114**, 990-995.
34. Q. Dou, M. L. Sha, H. Y. Fu, G. Wu. *J. Phys. Condens. Mat.* 2011, **23**, 175001-17009.
35. S. A. Kislenko, I. S. Samoylov, R. H. Amirov. *Phys. Chem. Chem. Phys*. 2009, **11**, 5584-5590.
36. M. Atilhan, S. Aparicio. *J. Phys. Chem. C* 2012, **116**, 12055-12065.
37. E. Soolo, D. Brandell, A. Liivat, H. Kasemägi, T. Tamm, A. Aablo. *J. Mol. Mod.* 2012, **18**, 1541-1552.
38. N. D. Patra, Y. Song, P. Kral,. *ACS Nano* 2011, **5**, 1798-1804.
39. M. Atilhan, S. Aparicio. *J. Phys. Chem. C* 2013, **117**, 22046-22059.
40. P. Wu, J. Huang, V. Meunier, B. G. Sumpter, R. Qiao. *ACS Nano* 2011, **11**, 9044-9051.
41. B. Qi, X. Xang, *Mat. Lett.* 2008, **62**, 980-983.
42. C. M. Maciel, E. E. Fileti. *Chem. Phys. Lett*. 2013, **568**, 75-79.
43. V. V. Chaban, C. Maciel, E. E. Fileti. *J. Solution Chem*. 2014, **43**, 1010-1031.
44. P. Nockemann, B. Thijs, K. Driesen, C. R. Jansenn, K. van Hecke, L. van Meervelt, S. Kossmann, B. Kirchner, K. Binnemans. *J. Phys. Chem. B* 2007, **111**, 5254-5263.
45. D. J. Couling, R. J. Bernot, K. M. Docherty, J. K. Dixon, E. J.Maginn. *Green. Chem.* 2006, **8**, 82-90.
46. Pernak, J. Syguda, A., Mirska, I. Nawrot, J. Pradzynska, A. Griffin, S. T., Rogers, R. Choline-Derivative-Based Ionic Liquids. *Chem. Eur. J.* 2007, 13, 6817–6827.
47. A. P. Lyubartsev, A. Laaksonen. *Comput. Phys. Commun*. 2000, **128**, 565-589.

48. U. L. Essmann, M. L. Perera, T. Berkowitz, H. Darden, H. Lee, L. G. Pedersen. *J. Chem. Phys*. 1995, **103**, 8577-8593.
49. M. Tuckerman, B. J. Berne, G. J. Martyna. *J. Chem. Phys*. 1992, **97**, 1990-2001.
50. S. Aparicio, M. Atilhan, N. Pala. *J. Chem. Phys.* 2013, **139**, 224502.
51. N. J. English, D. A. Mooney, S.O'Brien. *Mol. Phys.* 2011, **109**, 625-638.
52. Y. Zhao, K. Dong, X. Liu, S. Zhang, J. Zhu, J. Wang. *Mol. Sim.* 2012, **38**, 172-178.
53. N. J. English, D. A.Mooney. *J. Phys. Chem. B* 2009, **113**, 10128-10134.
54. N. J. English, D. A.Mooney. *Phys. Chem. Chem. Phys.* 2009, **11**, 9370-9374.
55. J. P. Perdew, K. Burke, M. Ernzerhof. *Phys. Rev. Lett*. 1996, **77**, 3865–3868.
56. http://www.home.uni-osnabrueck.de/apostnik/download.html. Accesed on January 16, 2014.
57. J. M Soler, E. Artacho, J. D. Gale, A. García, J. Junquera, P. Ordejón, D. Sánchez-Portal. *J. Phys. Condens. Matter*. 2002, **14**, 2745-2779.
58. N. Troullier, J. L.Martins. *Phys. Rev. B* 1991, **43**, 1993–2006.
59. J. Kürti, J. Koltaik V. Zólyomi, S. Pekker *Phys. Stat. Sol*. 2009, **246**, 2618-2621.
60. A. Z. Alzanrani. *ISRN Condensed Matter Physics*. 2012, **2012**, 208234.
61. M. J. Frisch, G. W. Trucks, H. B. Schlegel, G. E. Scuseria, M. A. Robb, J. R. Cheeseman, G. Scalmani, V. Barone, B. Mennucci, G. A. Petersson, H. M. Nakatsuji, H. Caricato, X. Li, H. P. Hratchian, A. F. Izmaylov, J. Bloino, G. Zheng, J. L. Sonnenberg, M. Hada, M. Ehara, K. Toyota, R. Fukuda, J. Hasegawa, M. Ishida, T. Nakajima, Y. Honda, O. Kitao, H. Nakai, T. Vreven, J. A. Montgomery Jr., J. E. Peralta, F. Ogliaro, M. Bearpark, J. J. Heyd, E. Brothers, K. N. Kudin, V. N. T. Staroverov, Keith, R. Kobayashi, J. Normand, K. Raghavachari, A. Rendell, J. C. Burant, S. S. Iyengar, J. Tomasi, M. Cossi, N. Rega, J. M. Millam, M. Klene, J. E. Knox, J. B. Cross, V. Bakken, C. Adamo, J. Jaramillo, R. Gomperts, R. E. Stratmann, O. Yazyev, A. J. Austin, R. Cammi, C. Pomelli, J. W. Ochterski, R. L. Martin, K. Morokuma, V. G. Zakrzewski, G. A. Voth, P. Salvador, J. J. Dannenberg, S. Dapprich, A. D. Daniels, O. Farkas, J. B. Foresman, J. V. Ortiz, J. Cioslowski and D. J. Fox. *Gaussian 09*, Revision D.01, Gaussian, Inc.: Wallingford, CT 2010.
62. R.F.W. Bader, *Atoms in Molecules: a Quantum Theory* Oxford University Press, Oxford, 1990.
63. A. E. Reed, L. A. Curtiss, F. Weinhold. *Chem. Rev*. 1988, **88**, 899-926.
64. F. Biegler-König, J. Schönbohm, D. Bayles. *J. Comput. Chem.* 2001, 22, 545-559.
65. B. E. Dunlap, R. J.Zope. *Chem. Phys. Lett.* 2006, **422**, 451-454.
66. S. Itoh, P. Ordejón, D. A. Drabold, R. M.Martin. *Phys. Rev. B* 1996, **53**, 2132-2140.
67. S. Aparicio, M. Atilhan. *J. Phys. Chem. B* 2012, **116**, 9171-9185.
68. R. Singh, J. Monk, F. R. Hung, *J. Phys. Chem. C* 2010, **114**, 15478.
69. S. Chen, G. Wu, M. Sha, S. Huang, J. Am. Chem. Soc., 2007, **129**, 2416–2417.
70. T. Ohba, V. V. Chaban, *J. Phys. Chem. B*, 2014, **118**, 6234.
71. S. Banerjee. *J. Chem. Phys.* 2013, **138,** 044318.
72. S. Aparicio, M. Atilhan, N.Pala. *J. Chem. Phys*. 2013, **139**, 224502.
73. M. Y. Amusia, A. S. Baltenkov, *Phys. Lett. A* 2006, **360**, 294-298.
74. J. P. Connerade, A. V. Slov'yov, *J. Phys. B*, 2005, **38**, 807.
75. S. Lo, A. V. Korol, A.V. Slov'yov, *J. Phys. B*, 2007, **40**, 3973.